# Reticle Defect Printability and Photoresist Modeling of Contact Structures

**Warren W. Flack, Dan Schurz, Richard Lee, Calvin Ho**

**Ultratech Stepper, Inc.**

**San Jose, CA 95134**

Over the past few years there has been a growing interest in using advanced image formation techniques to enhance optical lithography resolution. Techniques such as Optical Proximity Correction (OPC) and phase shifting involve changes in reticle manufacturing which increase the printability risk of small reticle defects and therefore impact wafer yields. There have been several experimental and simulation studies on the printability of sub-half micron defects using both reduction and 1X photolithography equipment. In general these studies have focused on the printability effects of line and space features. However, OPC is frequently implemented to control the size and shape of contact structures.

This study was performed to gain a better understanding of the behavior of contact hole defects in a 1X lithography system using both a moderate and a high contrast photoresist. A test reticle was created with 0.72 μm contact holes containing edge, corner and isolated central defects in programmed sizes from 0.15 to 0.4 μm, and exposed on a submicron 1X stepper. Printability was determined by measurement of the normalized area of the contact (NCA).

Reticle defect printability of the contact structures was modeled for each photoresist using a three-dimensional (3D) optical lithography simulation tool. The experimental NCA data was compared to modeled results to validate the simulator. Cross sectional contact simulations were then prepared to show the relative impact on the placement of the defect in the contact structure. Both the simulation and the experimental results show the relative sensitivity of the two photoresists to the printability of defects in the contact hole structure. This analysis enhances the understanding of the criticality of defect sizes in contact arrays and allows users to predict defect printability issues for new photoresists.

**Key Words:** sub-half micron defects, contacts, reticle defect printability, defect simulation

## 1.0 INTRODUCTION

Several simulation and experimental studies have been completed which seek to establish general rules and conditions pertaining to the printability effects of sub-micron defects in reduction lithography systems [1, 2]. The study of defect printability has been expanded to include 1X lithography systems since they are widely used in mix-and-match applications [3, 4]. In both of these studies, the effects of a series of clear and opaque reticle defects were observed on wafers exposed using a 1X projection stepper [3]. Similarities were found in defect behavior pertaining to defect size (area), proximity to line edge, and defect tone in both reduction systems and 1X projection systems.

Most of these defect studies have been conducted on line/space patterns of varying pitch. Studies of the behavior of defects on contact holes have typically been done with transmission or transparent reticle defects and especially on 5X reduction lithography systems [5, 6, 7]. Schuda et. al. found that on a 5X reduction system, opaque isolated center defects in contacts have greater printability than those on the edge [5]. Similar results were observed by Kawahira et. al. in their work to develop an industry standard defect test reticle for inspection equipment and reduction steppers [6]. One of the purposes of this study is to empirically confirm similar contact defect behavior in a 1X projection system. With sufficient similarities between the two lithography systems, it would be possible to extend the prediction of the behavior of transmission type defects through the use of simulations.

One area that has not been thoroughly examined is the impact of photoresist contrast on the printability of contact defects. Frequently, special photoresist formulations are used for contact level lithography in order to increase contact resolution. In an earlier experiment, Wiley showed no significant differences in defect behavior with Shipley Microposit[®] 1400-27 and Shipley Microposit[®] 1813 [8]. However, these are both relatively low contrast materials with similar sensitizer properties. In a simulation study, Karklin predicted that a higher contrast photoresist affects the printability of contact holes by allowing for wider process windows [9]. However, there was no experimental verification of these predictions. In this study, experimental results are used to validate the 3D simulation work. This supports the simulation of defect behavior for new photoresists in a 1X lithography process.

A thorough understanding of contact defect printability can be used by lithographers to define cost-effective reticle quality specifications for their production lines and chip designs. Mask manufacturers can benefit by not having to inspect for and repair defects that are below the margins of printability. In addition, defect simulation can be used to predict the effect of known defects on existing reticles to determine if they can be safely used for manufacturing [10].

## 2.0 EXPERIMENTAL METHODS

### 2.1 Reticle Design and Manufacture

The reticle design for this experiment was based on a metal layer for a 4 Megabit (Mb) DRAM shrunk down to a 0.65 μm design rule that is representative of a 64 Mb process. The memory core areas were removed and replaced with clear contact arrays consisting of 0.80 μm square contacts at a 3.2 μm pitch in both the x and y directions. This design allowed for a defect printability study utilizing a standard production type reticle. Square defects were added to two unique dice that could be compared to similar, defect free dice in a 9 by 9 array.

Four types of square defects were implemented: opaque center edge, opaque corner, opaque isolated center, and clear edge extensions, as shown in Figure 1. Two sets of opaque square defects in CAD sizes of 0.20, 0.25, 0.30, and 0.40 μm were placed in the array. One set was attached to the edges, and another set was placed in the contact centers. The third set of opaque squares in CAD sizes of 0.15, 0.20, 0.25, 0.30, and 0.40 μm were added to the contact corners. A set of clear extension defects at the same sizes as the third set, were centered on contact edges. In total 18 defects were added as a separate pattern file to two of the dice within each field.

The reticle was written on a MEBES 4500 using a high resolution PBS resist. There was no data biasing applied to the design data and CDs were held to within ±0.03 μm of a nominal 0.65 μm chrome line. All reticle defects were measured and CDs verified on a Hitachi S-7280H low voltage metrology SEM. All subsequent defect sizes reported in this study refer to the measured size on the reticle, not the CAD drawn size.

### 2.2 Processing Conditions

Multiple 200 mm silicon wafers were used for this study. All wafers were vacuum-baked and HMDS primed prior to photoresist coating. Two photoresists manufactured by Japanese Synthetic Rubber (JSR) were used throughout this investigation. JSR ix500EL® is a moderate contrast photoresist and JSR ix875® is a very high contrast photoresist. Experimental swing curves indicated an optimal photoresist thickness of 0.98 μm for 0.65 μm resolution. This $E_{max}$ location on the swing curve provides maximum process latitude. Both photoresists were coated to the 0.98 μm target thickness using the process and equipment described in Table 1. Photoresist coating thickness and uniformity were verified on a Prometrix FT700 film measurement system. Photoresist thickness uniformity was held to ±100Å across the entire lot of wafers. The post exposure bake and develop processes are shown in Table 2.

### 2.3 Lithography Equipment

All lithography was performed on an Ultratech Stepper Saturn Wafer Stepper® lithography system. The Ultratech stepper is based on the 1X Wynne-Dyson lens design employing broadband i-line illumination from 355 to 375 nm [11]. The Ultratech Saturn has a NA of 0.365, partial

coherence ($\sigma$) of 0.50 and is specified at 0.65 $\mu$m resolution, with 1.5 $\mu$m depth of focus (DOF), and a field size of 44 by 22 mm. Exposure uniformity was verified prior to collecting the experimental data and was found to be 1.2 percent across the entire field. Multiple wafers were exposed in a focus and exposure array as illustrated in Figure 2. Nominal exposure dose was determined by measuring dense 0.72 $\mu$m contact patterns with a Hitachi S-7280H low-voltage SEM. A 35 percent threshold criteria was selected to determine the contact CD. Nominal exposure dose was determined to be 280 mJ/cm$^2$ for the JSR ix500 and 260 mJ/cm$^2$ for the JSR ix875 with all data collected at best-focus.

### 2.4  Simulation

Optical microlithography simulation programs have been shown to provide results representative of actual production processes. Given the simulation is well matched to the experimental lithography process, an extensive number of defect types may be easily investigated. Solid-C$^{®}$, a commercially available optical lithography simulation program, was used to generate all of the modeling results presented in this study. The JSR ix500 and JSR ix875 photoresist parameters used as inputs for the simulation program are shown in Table 3. Note that the developer selectivity term **n** for the JSR ix875 is much larger than the JSR ix500. This is an indicator that the JSR ix875 has a higher contrast than the JSR ix500. The Saturn wafer stepper parameters used as inputs for the simulation program are shown in Table 4.

Matching lithography simulation to experimental results has been investigated in other works [12]. One matching procedure involves comparison of simulated and actual swing curves. Thorton and Mack determined that adjustments could be made to the photoresist **C** parameter and photoresist index of refraction to match the swing curves. These adjustments are employed to compensate for differences in relative photoresist thickness measurements and exposure dose calibration differences.

The approach used in this study involves matching process latitude windows. Experimental focus/ exposure matrices were obtained from which Bossung plots were generated. The plot of the process window for each photoresist was then compared to simulated results generated with the parameters included in Tables 3 and 4. The experimental and modeled plots are very similar in terms of DOF and exposure latitude. This agreement of process windows gives an excellent indication of overall matching. The details of this matching technique are described in a previous study [13].

## 2.5  Data Analysis

Since the defect sizes used in this study are below the minimum resolution of the Saturn stepper, the response was defined as the change in the normalized contact area (NCA) printing in the photoresist:

$$NCA = \frac{ECA}{RCA} \tag{1}$$

The experimental contact area (ECA) is the area of the printed contact containing the defect. The reference contact area (RCA) was determined by measuring neighboring contacts on the wafer that did not contain a defect. For simplicity of data analysis, all contacts were assumed to be ellipsoidal. This allowed the contact area to be determined by measuring only two parameters, the long and short axis. However, this simplification does create a source of measurement error and will be discussed in detail in section 3.3.2.

The changes in the NCA for the four defect types illustrated in Figure 1 were measured over a range of defect sizes. The actual defect sizes were determined by measuring the contact dimensions on the reticle. Multiple measurements were made in both the x and y axis to determine the average side of the square defect. Since the actual defects resolved on the reticle are not always square, this introduces another source of measurement error that is discussed in detail in section 3.3.2.

Simulation data was generated for each of the four defect types over the experimental range of defect sizes. The area of the modeled contacts was also assumed to be ellipsoidal. This data provides a mechanism to validate the simulation results by providing a comparison with the experimental defect data.

# 3.0  RESULTS AND DISCUSSIONS

## 3.1  Visual Comparison of Experimental and Simulation Results

A visual comparison of experimental and simulation results for two representative defects was performed. Figure 3a shows the layout of a 0.72 μm contact with a 0.25 by 0.25 μm opaque center edge defect. Superimposed on the layout is the gray, elliptical outline of the simulated JSR ix500 photoresist contour at a 35 percent theshold. Note that the centerline of the predicted contact is slightly off-center from the layout away from the center edge defect. The simulated contact clearly has an ellipsoidal shape with the vertical CD smaller than the horizontal CD. Figure 3b shows the same programmed defect in a contact on the reticle. The black outline in Figure 3b was placed to help visualize the CAD layout due to the low contrast of the SEM micrograph. The experimental contact image on the wafer with JSR ix500 photoresist is shown in Figure 3c. The

experimental contact clearly shows a similarly heliopolis shape as in the photoresist contour simulation in Figure 3a.

Figure 4a shows a 0.72 μm contact with a 0.25 by 0.25 μm clear extension defect. Again, the resultant JSR ix500 photoresist contour is slightly off-center, but shifted up in the direction of the extension defect. The extension defect increases the vertical CD which results in a substantially larger contact area than the contact with the opaque center edge defect shown in Figure 3a. Figure 4b shows the contact with the clear edge extension defect as it appears on the reticle. Again, the black outline was placed to help visualize the CAD layout due to the low contrast of the SEM micrograph. Finally, Figure 4c shows the experimental contact on the wafer with JSR ix500 photoresist which clearly shows the increased vertical CD.

A comparison of Figures 3c and 4c shows the large impact on contact size that can result from a reticle defect. The different sizes qualitatively match the simulated contacts in Figures 3a and 4a. This suggests a good visual match between the experimental and simulated results for the JSR ix500 photoresist.

## 3.2  Simulated Cross Sectional Contacts

A clear way to visualize the effect of different types of defects on contact printability is to look at cross sections. Since the contact array used in this study was not designed to support cross sectional analysis, it is necessary to look at simulated cross sections as shown in Figures 5 and 6. These figures show the differences between simulated contacts with no defect, an opaque corner defect, an opaque center edge defect, and an opaque isolated center defect using JSR ix500 photoresist (Figure 5) and JSR ix875 photoresist (Figure 6). These figures are simulations of a 0.72 μm contact with a 0.25 μm square defect at a photoresist thickness of 0.98 μm.

Figures 5a shows a defect free contact in JSR ix500 photoresist. It is apparent that the contact has excellent CD control and very steep sidewall angles. The addition of a corner defect (Figure 5b), center edge defect (Figure 5c) and a isolated center defect (Figure 5d) results in progressively decreasing contact quality. Note that the contact with the corner defect (Figure b) appears to have the least effect on the contact area while the contact with the isolated center defect (Figure d) has the most effect on the contact. While the corner defect and edge center defects reduce the area and sidewall quality of the contact, the structure is still open at the bottom of the photoresist. The contact with the isolated center defect clearly is not open and is reminiscent of an under-exposed contact.

Figure 6 shows the same contact structures for the JSR ix875 photoresist. It is interesting that there is little observable difference between the two types of photoresist. Both photoresists provide near identical contact areas at the bottom surface. However, the JSR ix875 photoresist does provide a better side wall due to its inhibition properties. This is evident from the concave side wall towards the top of the photoresist profile. Another consideration is that the simulations for both photoresists were generated at best focus conditions. It is expected that the difference in

contrast between the photoresists would be more apparent at the extremes of the focus and exposure process window.

### 3.3  Experimental and Simulation Defect Results

#### 3.3.1 Impact of Defect Types on Printability

Figure 7 shows simulated and experimental defect printability for opaque edge center, opaque corner, opaque isolated center and clear extension defects. The simulated and experimental contact area data was analyzed as previously discussed in section 2.5. Figures 7a and 7b show the experimental data for the JSR ix500 and JSR ix875 photoresists respectively. A NCA value of 1 indicates that the defect had no impact on the size of a contact. Clearly the edge extension defect increases the NCA while the corner and edge center defect deceases the NCA. The edge center defect has a larger affect on the NCA than the corner defect for both photoresists. Note that the opaque isolated center defect is not included in either figure. This is because the isolated center defects were either unresolved or bridged on the reticle. Thus, insufficient data was available for inclusion in the experimental results.

Figures 7c and 7d show the simulated contact data for the JSR ix500 and JSR ix875 photoresists respectively. Here the isolated center defect has the largest impact on NCA while the edge center and corner defects have similar but smaller effects. For the JSR ix500 photoresist, an isolated center defect size between 0.10 and 0.15 µm will change the NCA by greater than 10 percent. Opaque defects located on the corner or center edge of the contacts have a similar effect between 0.20 and 0.25 µm. Clear extensions do not begin to change the NCA by greater than 10 percent until they are larger than 0.25 µm.

For the high contrast JSR ix875 photoresist, a more immediate effect in NCA is observed as defect size increases for all of the opaque defect types (Figure 7d). These defects begin to change NCA by greater than 10 percent when they reach between 0.15 and 0.20 µm. The isolated center defects up to 0.25 µm show behavior similar to the edge and corner opaques. Conversely, the clear extension defects began to affect NCA at the slightly smaller size of 0.20µm, compared to the 0.25 µm in the moderate contrast photoresist. These results are expected since the higher contrast photoresist effectively increases resolution by providing a lower k value which makes it more susceptible to printing both clear and opaque defects.

#### 3.3.2 Measurement Error Sources

Several factors need to be considered when discussing the experimental and simulation defect results presented in section 3.3.1. First, the contact defects were added to a reticle originally designed to investigate defect behavior on line/space pairs. As a result, the CDs on the reticle were specified for a 0.65 µm line. Consequently, the contacts designed at 0.80 µm were actually measured at 0.72 µm on average on the reticle.

Square defect sizes less than 0.30 µm were difficult to resolve and typically produced contacts that were irregularly shaped. For all of the reticle data in section 3.3.1, the defect sizes are described by a single parameter, the length of a side of a square defect. This value was determined by averaging multiple contact measurements in both the x and y axis as described in section 2.5. In contrast, the defects used in the simulations were all perfect squares. The disparity between actual reticle defect size and shape versus the simulated defects is a primary cause of differences between the experimental and the simulated NCA results.

Another source of error is in the measurement of the contacts printed on the wafer. For simplicity of data analysis, all contacts were assumed to be ellipsoidal. This allowed the NCA to be determined by measuring only two parameters, the long and short axis. However, contacts were frequently observed to be more irregular in shape. Therefore, the NCA may have been overestimated or underestimated depending on the actual shape.

### 3.3.3 Quantitative Comparison of Experimental and Simulation Results

The contact corner defects produced the most consistent reticle measurements which suggested that the measurement error sources were smallest for this type of defect. As a result, corner defects were selected to quantitatively compare the simulated and experimental results.

Figure 8 shows a comparison of the simulated and experimental results for opaque corner defects for both the JSR ix500 and ix875 photoresists. For the JSR ix500 photoresist (Figure 8a), the experimental defects appear to reduce the NCA at a much smaller defect size than predicted by the simulation. The JSR ix875 (Figure 8b) shows a higher correlation between the experimental and simulation data. This suggests that there is less experimental error in measuring the contacts printed in the JSR ix875 than the JSR ix500. This is probably due to the difference in contrast between the two materials. It is also interesting to note that the NCA of the JSR ix875 photoresist shows a larger response to small defect sizes than the JSR ix500. Again, this is probably due to the higher contrast photoresist effectively increasing the resolution by providing a lower k value and making it more susceptible to printing smaller defects.

## 4.0 CONCLUSIONS

This study incorporated a series of contacts on a 1X reticle containing several different programmed defect types and tones added to the contact edges, corners and centers. The small sizes of these programmed defects made it difficult to accurately measure the size of contacts on the test reticle. This introduced a significant error source which is evident when comparing experimental and simulated results. The measurement error emphasizes both the difficulty in and the importance of developing an industry standard for defect measurement as has been proposed by SEMI Japan [6].

Empirical data taken from earlier studies in line/space pairs and this current study of contacts, have demonstrated the viability of using 3D simulation as a prediction tool for reticle defect behavior of different process layers in 1X lithography systems. The results of the photoresist comparison also indicate the value of simulation to predict lithography results for process changes. They also confirm the expectation that higher contrast photoresists exhibit a higher sensitivity to defect printability in 1X.

With the development of a defect measurement standard and continued improvements in measuring capability of reticle defect inspection systems, it will be possible for photomask manufacturer's to provide information on irrepairable defects to customers to simulate in their respective processes to determine printability. Simulations can also be used to provide mask makers with defect specifications tuned to particular process layers and parameters, thereby reducing the cost of incorrectly specifying reticles.

## 5.0  ACKNOWLEDGEMENTS

## 6.0  REFERENCES

1. J. N. Wiley, J. A. Reynolds, "Device Yield and Reliability by Specification of Mask Defects," *Solid State Technology*, **36** (7), July 1993.

2. P. Yan, J. Langston, J. Neff, R. Chatterjee, "Mask Defect Printability and Wafer Process Critical Dimension Control at 0.25 μm Design Rules," *Bacus News*, **12** (1) Jan 1996.

3. D. Schurz et. al., "Sub-Micron Mask Defect Detectability and Printability at 1X Reticle Magnification," *Symposium on Photomask Technology and Management Proceedings*, SPIE **2884** (1996).

4. D. Schurz et. al., "The Printability of 1X reticle Defects for Submicron Design Rules," *Symposium on Photomask Technology and Management Proceedings*, SPIE **3236** (1997).

5. S. Schuda, S. Y. Shaw, S. Palmer, "Printability Study of Opaque and Transparent Defects Using Standard and Modified Illumination," *Optical/Laser Microlithography VIII Proceedings*, SPIE **2440** (1995).

6. Hiroichi Kawahira, Yoshiki Suzuki, "SEMI Standards Programmed Defect Masks and Its Applications for Defect Inspection," *Integrated Circuit Metrology, Inspection, and Process Control IX Proceedings*, SPIE **2439** (1995).

7. L. Zurbrick, S. Schuda, J. Wiley, "Effects of Transparent and Transmission Reduction Reticle Defects," *Optical/Laser Microlithography VIII Proceedings*, SPIE **2440** (1995).

8. James N. Wiley, "Process Effects in 5X Reticle Defect Printability," *Ninth Annual Symposium of the Bay Area Chrome Users Society Proceedings*, (1989).

9. L. Karklin, "A Comprehensive Simulation Study of the Photomask Defects Printability," *Symposium on Photomask Technology and Management Proceedings*, SPIE **2621** (1995).

10. B. Riester, S. Steuber, F. Gans, "Printability Simulation of Reticle Defects For Predictive Reticle Qualification," *Olin Microlithography Seminar, Interface'97 Proceedings,* (1997).

11. G. Flores, W. Flack, L. Dwyer, "Lithographic Performance of a New Generation i-line Optical System," *Optical/Laser Lithography VI Proceedings*, SPIE **1927** (1993).

12. S. Thorton and C. Mack, "Lithography Modeling Tuning," *Optical Microlithography IX Proceedings*, SPIE **2726** (1996).

13. W. Flack et. al. "Simulation of Subhalf-Micron Mask Defect Printability at 1X Reticle Magnification," *Integrated Circuit Metrology, Inspection and Process Control XI Proceedings*, SPIE **3050** (1997).

| Process Step | Parameters | Equipment |
|---|---|---|
| Vacuum Bake, HMDS vapor-prime | | YES LP-3 Oven |
| Photoresist Coat | 9 second radial dispense at 1000 rpm<br>6 second spin at 3080 rpm<br>25 second spin at 1000 rpm | MTI Flexifab Track |
| Softbake | 60 seconds at 100°C<br>Hard-contact | MTI Flexifab Track |

**Table 1:** Photoresist process and equipment used in this study.

| Process Step | Parameters | Equipment |
|---|---|---|
| Postexposure bake | 60 seconds at 120°C (JSR ix500)<br>60 seconds at 110°C (JSR ix875)<br>Hard-contact | MTI Flexifab Track |
| Develop | 60 second single puddle,<br>PD-523 developer at 25°C<br>20 second DI water rinse<br>Spin dry | MTI Flexifab Track |

**Table 2:** Post exposure bake and develop processes used in this study.
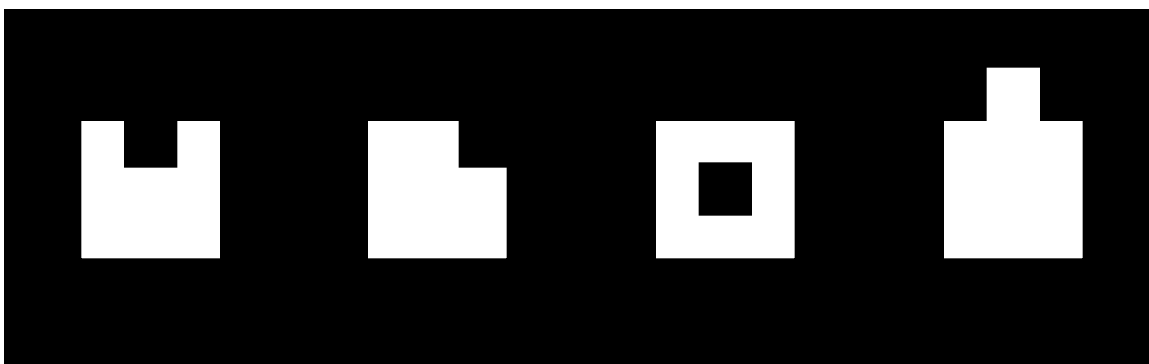


**Figure 1:** Illustration of the types of contact defects used in this study. From left to right are opaque edge center, opaque corner, opaque isolated center and clear edge extension defects.
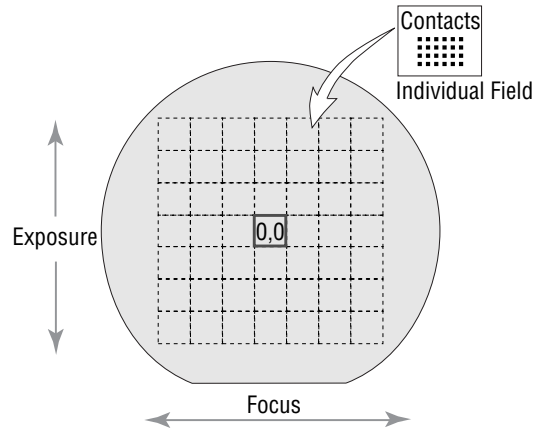
**Figure 2:** Wafer layout for exposure of the defect test reticle.

| Parameter | JSR ix875 | JSR ix500 |
|---|---|---|
| Photoresist softbake temperature ($^o$C) | 100 | 100 |
| Photoresist bake time (seconds) | 60 | 60 |
| Photoresist thickness (µm) | 0.98 | 0.98 |
| Photoresist A parameter (µm$^{-1}$) | 0.810 | 0.5506 |
| Photoresist B parameter (µm$^{-1}$) | 0.050 | 0.0656 |
| Photoresist C parameter (cm$^2$/mJ) | 0.012 | 0.0141 |
| Photoresist index of refraction | 1.70 | 1.70 |
| PEB diffusion length (µm) | 0.060 | 0.065 |
| PEB thickness loss (µm) | 0 | 0 |
| Maximum develop rate (nm/s): $R_{max}$ | 85 | 85 |
| Minimum develop rate (nm/s): $R_{min}$ | 0.02 | 0.0091 |
| Developer selectivity: n | 9.00 | 5.8 |
| Theshold PAC concentration: m | 0.36 | 0.06 |
| Develop time (seconds) | 60 | 60 |

**Table 3:** Constant simulation input parameters for the photoresist processing.

| Parameter | Value |
|---|---|
| Reduction factor | 1X |
| Wavelength (nm) | 365 |
| Numerical Aperture (NA) | 0.365 |
| Partial Coherence ($\sigma$) | 0.50 |
| Defocus setting (µm) | 0 |

**Table 4:** Constant simulation input parameters for the lithography system.

0.72 um

0.25 um
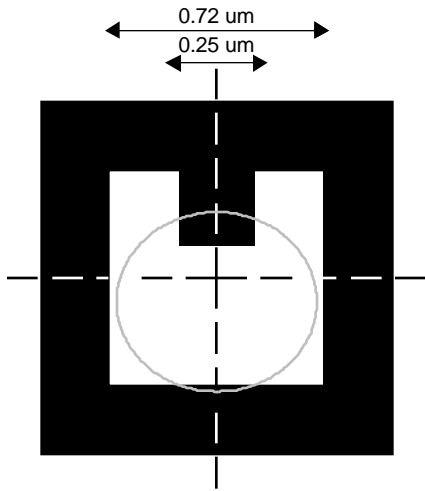
**3(a)** Layout of contact edge center defect
with photoresist simulation contour.

0.72 um

0.25 um

**4(a)** Layout of contact clear extension
defect with photoresist simulation contour.

**3(b)** SEM of contact on reticle.
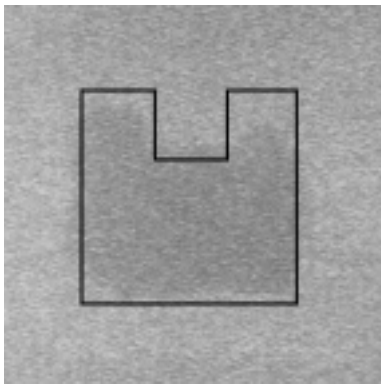
**4(b)** SEM of contact on reticle.
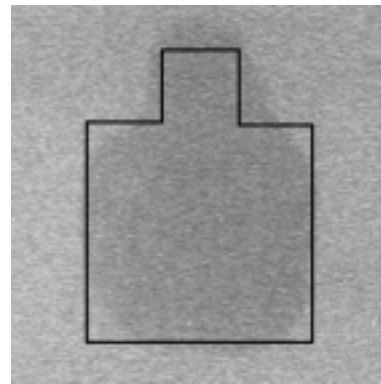
**3(c)** SEM of contact on wafer.
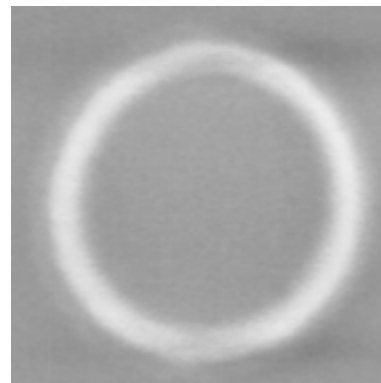
**4(c)** SEM of contact on wafer.

**Figures 3 and 4:** Comparisons of a chrome edge defect (Figure 3) and a clear extension defect
(Figure 4) on the wafer and reticle. The photoresist is JSR ix500 at a thickness of 0.98 μm. All
micrographs are at 40,000X on a Hitachi S-7280H SEM.
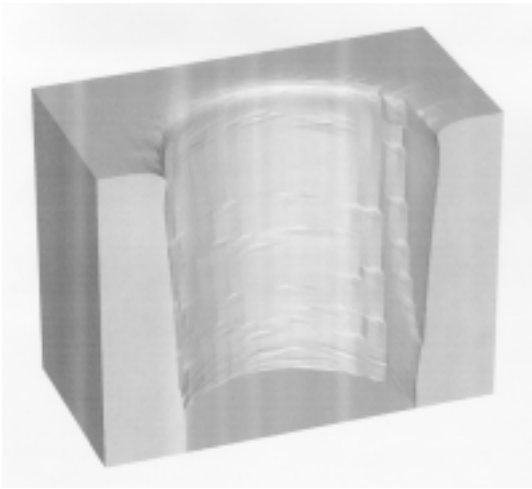
**(a)** Cross sectional contact with no defect.
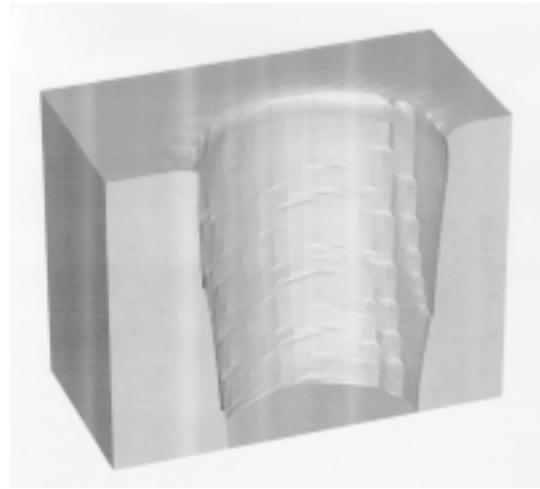


**(b)** Cross sectional contact with an opaque corner defect.
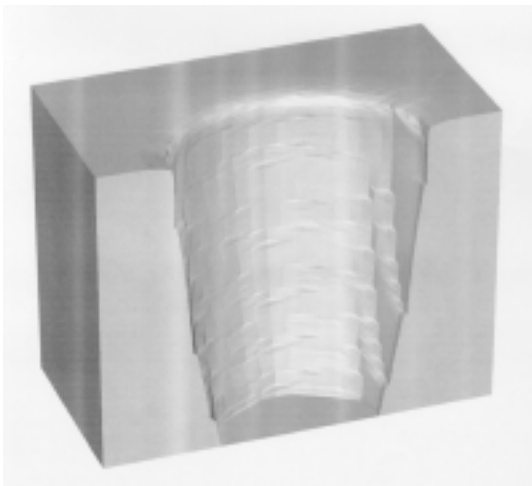


**(c)** Cross sectional contact with an opaque edge center defect.
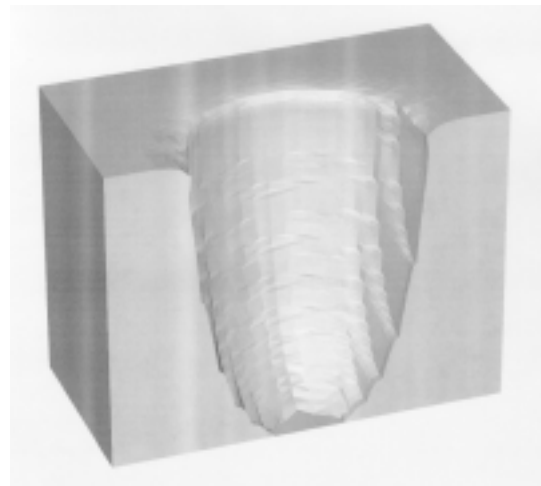


**(d)** Cross sectional contact with an opaque isolated center defect.

**Figure 5:** Simulated cross sections of 0.72 μm contact in 0.98 μm of JSR ix500 photoresist. Each defect is 0.25 μm square and placed in the contact as shown in Figure 1.
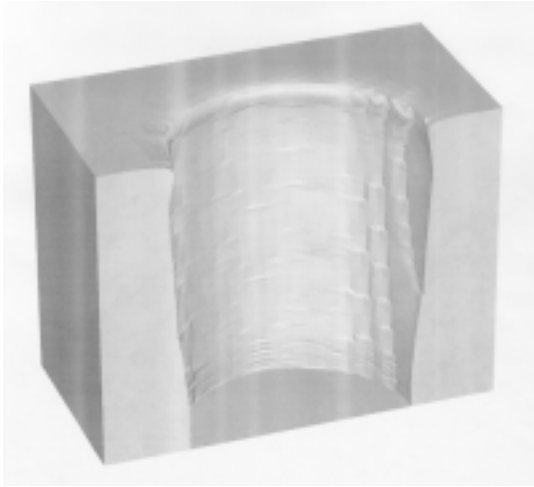
**(a)** Cross sectional contact with no defect.
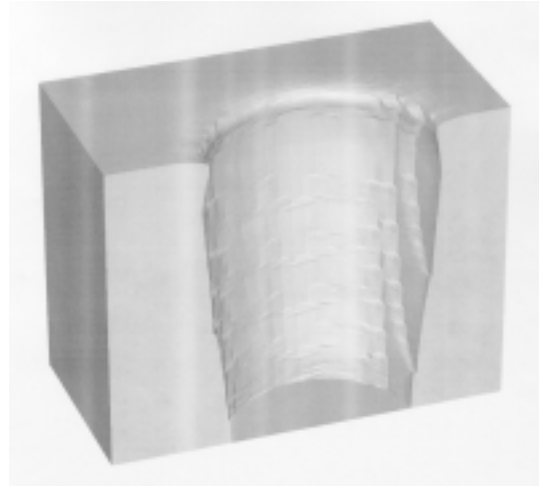


**(b)** Cross sectional contact with an opaque corner defect.
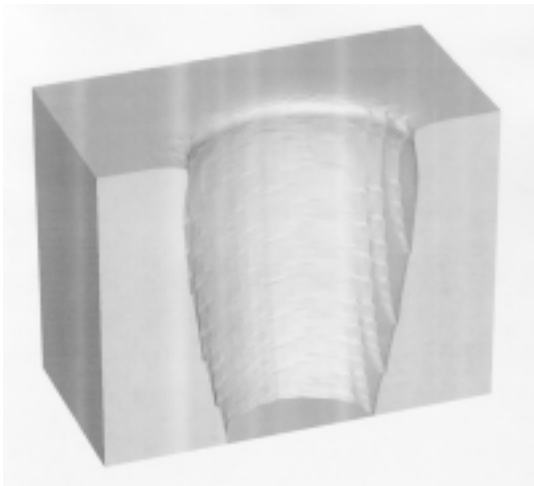


**(c)** Cross sectional contact with an opaque edge center defect.
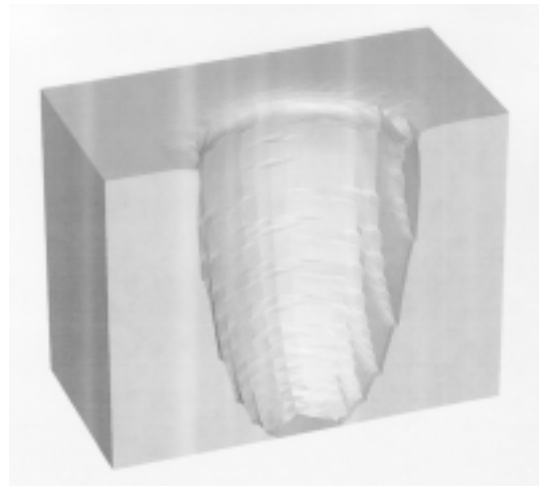


**(d)** Cross sectional contact with an opaque isolated center defect.

**Figure 6:** Simulated cross sections of 0.72 μm contact in 0.98 μm of JSR ix875 photoresist. Each defect is 0.25 μm square and placed in the contact as shown in Figure 1.
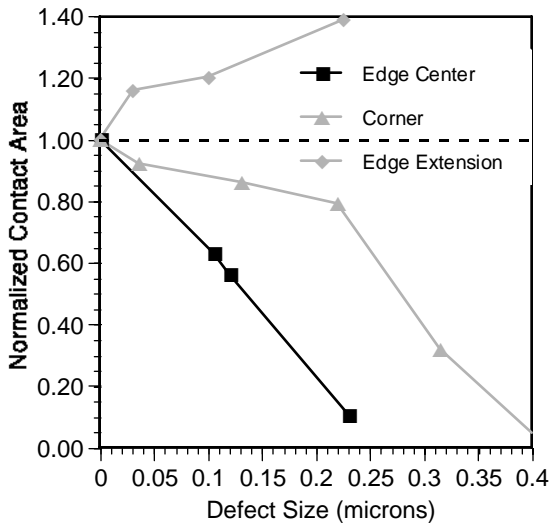
**(a)** Experimental data for JSR ix500.
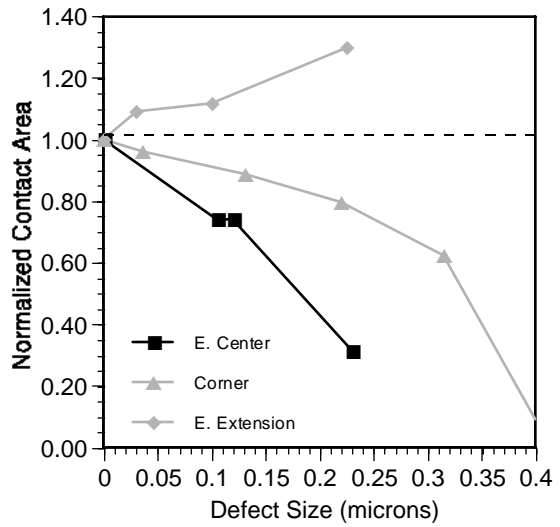
**(b)** Experimental data for JSR ix875.
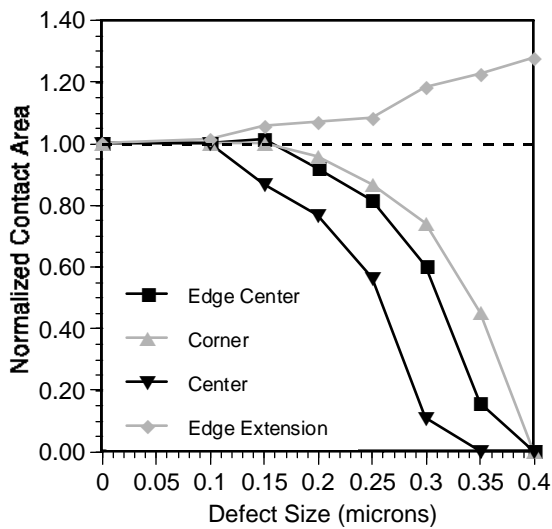
**(c)** Simulation data for JSR ix500.
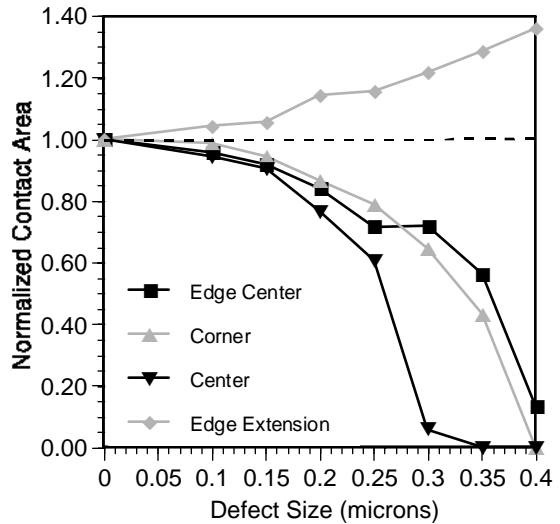
**(d)** Simulation data for JSR ix875.

**Figure 7:** Plot of normalized contact area (NCA) versus defect size for two types of photoresists. The contact size is 0.72 μm and the opaque defects are on the contact edge, the contact corner and isolated center of the contact. The clear defect is an extension on the contact edge. The response is the NCA where a value of 1 indicates no impact on the contact size.
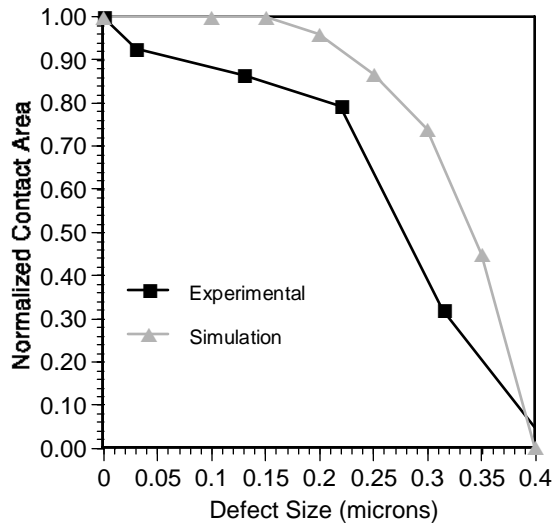
**(a)** Comparison of simulated and experimental corner defect data for JSR ix500.
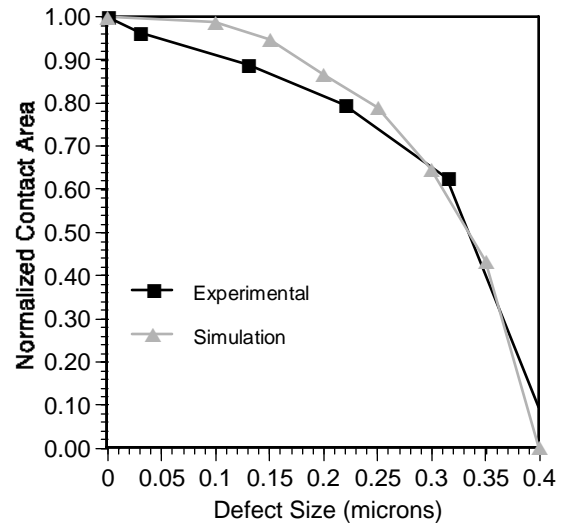
**(b)** Comparison of simulated and experimental corner defect data for JSR ix875.

**Figure 8:** Plot of normalized contact area (NCA) versus defect size for two types of photoresists. The contact size is 0.72 μm and the opaque defect is in the corner of the contact. The response is the NCA where a value of 1 indicates no impact on the contact size.